Alexandria Journal of Science and Technology

Article

Molecular dynamics simulations of *s*-triazine-based MMP-10 inhibitor with ferroptosis induction capacity and potent anti-colorectal cancer activities

Omar A. Soliman [1,2], Christine A. Morcos [3,*], Nesreen S. Haiba [4], Rafik W. Bassily [3], Marwa M. Abu-Serie [5], Mohamed Teleb [6], Sherine N. Khattab [3]

[1] *Department of Clinical Pharmacy, Alexandria University Main Teaching Hospital, Alexandria, Egypt.*

[2] *Department of Human Genetics, Medical Research Institute, Alexandria University, Alexandria, Egypt.*

[3] *Chemistry Department, Faculty of Science, Alexandria University, Alexandria 21321, Egypt.*

[4] *Department of Physics and Chemistry, Faculty of Education, Alexandria University, Egypt.*

[5] *Medical Biotechnology Department, Genetic Engineering and Biotechnology Research Institute, City of Scientific Research and Technological Applications (SRTA-City), Egypt.*

[6] *Department of Pharmaceutical Chemistry, Faculty of Pharmacy, Alexandria University, Alexandria 21521, Egypt.*

[*] *Correspondence Address:*

Christine A. Morcos: Chemistry Department, Faculty of Science, Alexandria University, Alexandria 21321, Egypt, Email address: christine.atef@alexu.edu.eg.

KEYWORDS: Molecular dynamics; MMPBSA; Docking; MMPs; Colorectal cancer; Triazine.

Received:
July 17, 2024

Accepted:
August 04, 2024

Published:
August 15, 2024

ABSTRACT: The present study explores the dynamic behavior and binding stability of a novel *s*-triazine-based MMP-10 inhibitor with ferroptosis induction capacity through comprehensive molecular dynamics (MD) simulations. The investigated compound, referred to as compound (I), demonstrated potent anti-colorectal cancer activities (HCT-116; IC_{50} = 0.018 µM). Mechanistically, the title compound (I) surpassed the reference MMPs inhibitor NNGH against MMP-10 (IC_{50} = 0.16 µM), depleted GSH in HCT-116 cells (relative fold decrement = 0.81) with modest GPX4 inhibition, and induced lipid peroxidation by 1.32 relative fold increment. Employing GROMACS program MD simulations were conducted for 100 ns to assess the complex's root mean square deviation (RMSD), root mean square fluctuation (RMSF), radius of gyration (Rg), solvent accessible surface area (SASA), ligand interaction network, contact frequency analysis, and Molecular Mechanics-Poisson Boltzmann Surface Area (MM-PBSA) binding free energy calculations aiming to elucidate the molecular tenets responsible for its anti-colorectal cancer activities. The results show that compound (I) has a stable and consistent interaction within the MMP-10 active site, which supports its promising inhibitory effect and prospective therapeutic application in colorectal cancer treatment. Colorectal cancer (CRC) is the third most frequent malignancy and the fourth most prevalent cause of cancer-related mortality.

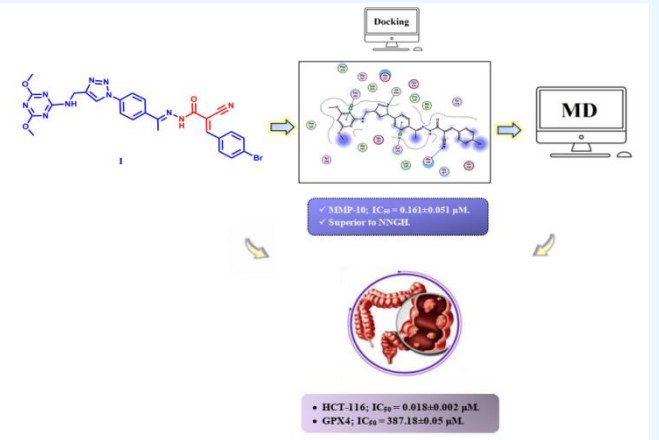

1. INTRODCTION

Molecular dynamics (MD) simulations can predict how each atom in a protein structure or any other molecular system will move over time [1]. These simulations thus can capture a wide variety of important biomolecular processes at femtosecond temporal resolution.

Online ISSN: 2974-3273

DOI: 10.21608/ajst.2024.305201.1042

In the area of drug discovery and at a qualitative level, simulations can guide the ligand optimization process by identifying the key interactions a ligand makes within the binding pocket, predicting rearrangements of the pocket induced by the ligand, and refining potential ligand poses [2,3]. At a quantitative level, simulation-based methods can provide more accurate estimates of ligand binding free energies than docking [4]. The Molecular Mechanics/Poisson-Boltzmann Surface Area (MM/PBSA) and Molecular Mechanics/Generalized Born Surface Area (MM/GBSA) methods, use MD simulation and rely on continuum solvent models rather than an explicit representation of water to offer accurate estimates of binding energies [5]. Different molecular dynamics simulation applications have been linked to the development of new drugs especially, anticancer agents [6].

Indeed, cancer research has concentrated on the extracellular matrix of the tumor microenvironment, which is primarily responsible for metastasis and proliferation [7,8]. Several different proteinases released into the extracellular matrix influence tumor progression events [9]. Among these matrix metalloproteinases (MMPs), a family of zinc-dependent endopeptidases, have been reported to be dysregulated in almost all human malignancies [10–12]. About twenty-six MMPs have been identified and classified as collagenases (MMP-1, -8, -13, −18), gelatinases (MMP-2, -9), stromelysins (MMP-3, -10), matrilysins (MMP-7, -26), membrane-type MMPs (MMP-14, -15, −16, −17, −24, −25), and others [13]. All members share an almost structurally similar catalytic domain consisting of three α-helixes and five β-sheets with the active-site zinc ion coordinated by three histidine residues, and five calcium ions. The domain is divided into *C*-terminal and *N*-terminal subdomains by a shallow cleft containing six binding pockets (S1, S2, S3, S1′, S2′ and S3′). The S1′ subsite is viewed as the selectivity pocket among various MMPs [14,15].

Several studies showed that MMPs as tumor microenvironment modulators and driving factors for cancer progression and patient prognosis [16–18]. It comes as no surprise then that MMPs are considered attractive anticancer targets. This is mirrored by the introduction of numerous MMP inhibitors over the past three decades [19–22]. Early inhibitors were designed as peptidomimetics or mimics of the MMPs' endogenous ligands combined with a hydroxamic acid cap as a zinc-binding group [22].

Although potent, these inhibitors failed in the clinic due to side effects [19], dose-limiting toxicity [23], and pharmacokinetic challenges [24] associated with the hydroxamic acid moiety [25,26]. The doubts about the suitability of hydroxamates as MMPs inhibitors then directed optimization studies to diversify the zinc-binding groups, therefore several non-hydroxamate MMP inhibitors were introduced [27,28].

Additionally, extensive efforts have been exerted to design and synthesize selective inhibitors. For MMP-10, potent inhibitors are rarely reported in the literature [29], despite being involved in different types of cancer [30–33], arthritis [34–36], atherosclerosis [37] and most recently Alzheimer's disease [38]. It is worth mentioning that sparing the hydroxamic acid ZBG while maintaining potency is indeed challenging. We recently described the optimization of new non-hydroxamate MMP-10/13inhibitors and the identification of a potent MMP-10 lead inhibitor (I) (**Figure 1**) surpassing the reference hydroxamate broad spectrum MMPs inhibitor *N*-hydroxy-2-[[(4-methoxyphenyl)sulfonyl](2-methylpropyl)amino]-acetamide (NNGH) [39]. This hit compound was also capable of inducing ferroptosis *via* GSH depletion in HCT-116 cells by a relative fold decrement of 0.81 and triggering lipid peroxidation by 1.32 relative fold increments. Inspired by these findings, we herein report a computational investigation of the hit compound (I) binding mode, stability, and dynamic behavior into MMP-10 active site *via* molecular dynamics simulations binding to gain more information on the structural determinants of activity in such lead compound.

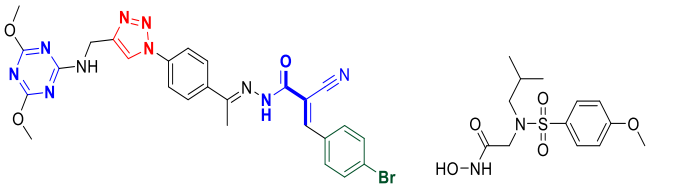

(I)

MMP-10; IC_{50} = 0.161±0.051 µM
GPX4; IC_{50} = 387.18±0.05 µM
HCT-116; IC_{50} = 0.018±0.002 µM

NNGH

MMP-10; IC_{50} = 0.623±0.011 µM

Figure 1. The chemical structures and biological activities of the triazine derivative (**I**) and the reference MMP-10 inhibitor *N*-hydroxy-2-[[(4-methoxyphenyl)sulfonyl](2-methylpropyl)amino]-acetamide (NNGH).).

2. Results and discussion

2.1. Chemistry

The copper-catalyzed click conditions were used to allow 4,6-dimethoxy-*N*-(prop-2-yn-1-yl)-1,3,5-triazin-2-amine to react with

(*E*)-*N*'-(1-(4-azidophenyl)ethylidene)-2-cyanoacetohydrazide

to produce the triazole derivative. Then, the desired product (I) [39] was produced by condensation of the active methylene group in the previously prepared compound with 4-bromobenzaldehyde in the presence of triethylamine in ethanol. (supplementary data, Scheme S1).

2.2. Docking

Docking the investigated compound (I) into the catalytic domain of MMP-10 was simulated by MOE 2019.0102 [40]. The enzymatic catalytic domain was retrieved from the protein databank; PDB ID: 1Q3A [41], prepared according to the MOE default settings and optimized as a monomer. The adopted protocol was first validated by reproducing most of the experimental interactions following redocking the co-crystallized ligand. The hit MMP-10 inhibitor (**I**) recorded lower binding free energy (ΔG = −9.04 kcal/mol) than that of the redocked NNGH (ΔG = −8.24 kcal/mol). This is consistent with the *in vitro* assay results. Its best presumed binding mode within the MMP-10 active site (**Figure 2**) showed that the scaffold could interact *via* the triazole ring with the active site zinc ion allowing the triazine core to display π-π stacking with the His221 and the linker phenyl ring to interact with Ser179 of the S1′ pocket.

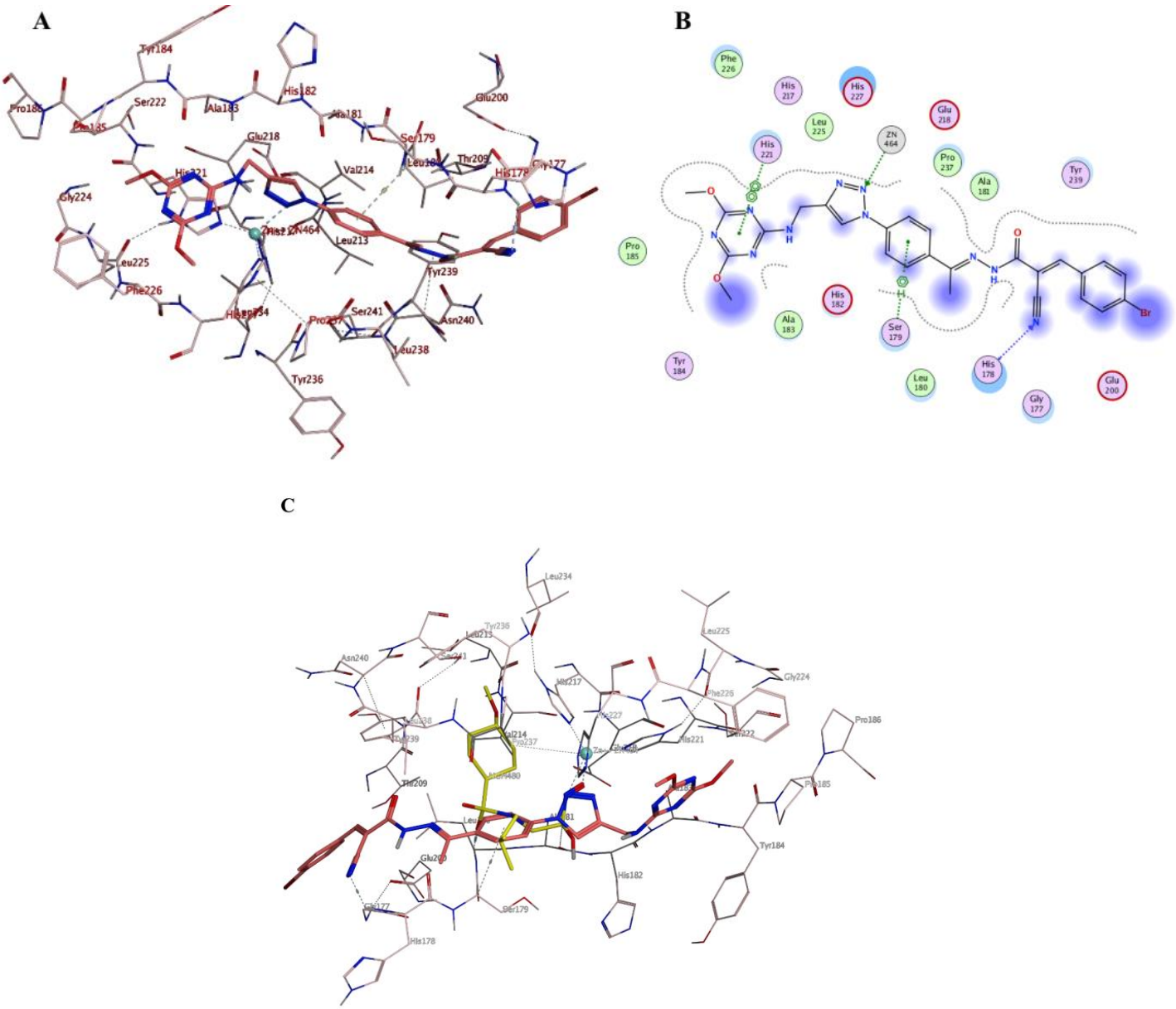

Figure 2. (A) 3D binding mode of the triazine derivative (I) (pink sticks), (B) 2D interactions of (I) in MMP-10 active site, (C) Overlay of the docked (I) (pink sticks) and the reference MMP inhibitor inhibitor *N*-hydroxy-2-[[(4-methoxyphenyl)sulfonyl](2-methylpropyl)amino]-acetamide (NNGH) (yellow sticks) in MMP-10 active site (PDB ID: 1Q3A). For 2D interactions; hydrogen bond interactions are illustrated as blue dotted arrows, π-H or π-π interactions are presented in green dotted lines, and zinc chelation is shown as red dotted line.

2.3. Molecular dynamics simulations

To study the dynamic behavior of the hit (I) into the active sites of MMP-10 (PDB ID: 1Q3A [41]), molecular dynamics simulations of the top-ranked docking pose were run for 100 ns at comparable physiological conditions employing the GROMACS program [42].

Analysis was performed in terms of root mean square deviation (RMSD), root mean square fluctuation (RMSF), radius of gyration (rGyr), ligand interactions network, and binding free energy (MMPBSA).

2.3.1. Root Mean Square Deviation (RMSD)

The RMSD plots of the complex were computed as a function of the simulation time to estimate the degree of deviation of each complex quantitatively relative to its initial behavior. Herein, the RMSD plot of the selected docking mode (**Figure 3A**) displayed RMSD ranging from approximately 1.5 to 2.5 Å. As illustrated, the RMSD increases rapidly within the first 10,000 ps, indicating significant structural deviations from the starting conformation. After this initial increase, the RMSD fluctuates around 1.5 Å, suggesting that the structure has reached a relatively stable conformation with minor variations. Around the 60,000 ps mark, the RMSD shows a noticeable increase, reaching a peak of approximately 2.5 nm. Following this peak, there is a gradual decrease in RMSD, stabilizing again around 1.5 Å towards the end of the simulation.

2.3.2. Root Mean Square Fluctuation (RMSF)

The RMSF was analyzed to study the side chain residue dynamics and local changes due to the inhibitor binding. The RMSF results complement the RMSD data by providing a more detailed view of residue-specific fluctuations. Calculations were based on '*C*-alpha' atoms using the GROMACS program. From the plot (**Figure 3B**), it is observed that most residues have an RMSF below 2 Å, indicating relatively stable behavior. However, there are significant peaks around residue numbers 250-270, where the RMSF exceeds 4 Å. This suggests that these residues experience higher flexibility and movement compared to the rest of the protein.

2.3.3. Radius of Gyration (Rg)

The Rg provides a measure of the compactness of a molecule. In the plot (**Figure 3C**), the Rg fluctuates around an average value of approximately 1.5 nm. There are minor variations in the Rg throughout the simulation. These fluctuations suggest that the protein undergoes minor conformational changes, but overall maintains a relatively consistent level of compactness. The calculated values were consistent with their respective RMSD.

2.3.4. The solvent accessible surface area (SASA)

The SASA plot over time (**Figure 3D**) indicates a fluctuating pattern with values oscillating between approximately 84 nm² and 94 nm². There is no apparent trend towards increasing or decreasing SASA, suggesting a dynamic equilibrium state. The rapid fluctuations observed throughout the simulation indicate significant conformational changes in the molecular system, reflecting the constant movement and rearrangement of the solvent molecules around the solute. Herein, the average SASA appears to be around 90 nm². Overall, the plot highlights the dynamic nature of the system and the continuous interaction between the solute and the surrounding solvent.

2.3.5. Ligand interaction network and contact frequency analysis

To further explore the ligand-protein binding nature and stability in the studied complex, ligand interactions network (**Figure 4**) and contact frequency (CF) (**Figure 5**) were analyzed over the whole simulation time for the simulated complex. Results (**Figures 4 and 5**) showed that compound (I) was in contact with many active site amino acids. The 2D interaction diagram showed that the ligand interacted with the key His178, His221, His227, Ala181, and others. The CF timeline further elucidates the stability and dynamics of these interactions over simulation time.

2.3.6. Molecular Mechanics-Poisson Boltzmann Surface Area (MM-PBSA) calculations

The MM-PBSA method was selected for rescoring the complexes being among the most employed force field-based methods. Accordingly, calculations were performed using *gmx. MMPBSA* software. Table 1 shows the Δ*G* binding energy, van der Waal, electrostatic, and polar solvation. MMPBSA revealed binding free energies ranged of -5.87±2.74 kcal/mol as shown in Table 1. Collectively, the outcome demonstrated that compound (I) remained in stable bound forms within MMP-10 active site during simulations and recommended its promising MMP-10 inhibitory activity.

3. Experimental

3.1. Chemistry

The title compound (**I**) was prepared according to the method reported by our group [39] and the spectra are detailed in the supplementary data (**Figures S1-S3**).

3.2. Docking

The MMP-10 binding mode analysis was performed employing MOE 2019.102 [40] as detailed in the supplementary data.

3.3. Molecular dynamics simulations

The input files for MD calculations were performed by the CHARMM-GUI solution builder [43–45] using CHARMM force field parameters as detailed in the supplementary data.

Conclusion

The detailed molecular dynamics simulations of the *s*-triazine-based MMP-10 inhibitor, compound (**I**), revealed significant insights into its binding mode and dynamic stability within the MMP-10 active site. The RMSD, RMSF, and Rg analyses confirmed the structural stability of the protein-ligand complex, while the SASA analysis indicated a dynamic equilibrium state with consistent solvation dynamics. The ligand interaction network and contact frequency analysis demonstrated stable hydrogen bonding and hydrophobic interactions, further substantiated by the MM-PBSA binding free energy calculations which indicated favorable binding affinity. These findings underscore the potential of compound (**I**) as a robust MMP-10 inhibitor with ferroptosis induction capacity, providing a foundation for its development as a potent anticancer therapeutic.

Acknowledgments

The authors thank the Science, Technology & Innovation Funding Authority (STDF), Cairo, Egypt, for funding this work through the Basic Sciences Research Grant (Proposal ID 48085). Also, the authors are grateful to The Bibliotheca Alexandrina Supercomputing facility (BA-HPC).

Declaration of competing interest (No conflict of interest)

The authors hereby declare that they have no competing financial interests or personal relationships that could have appeared to influence the work reported in this paper.

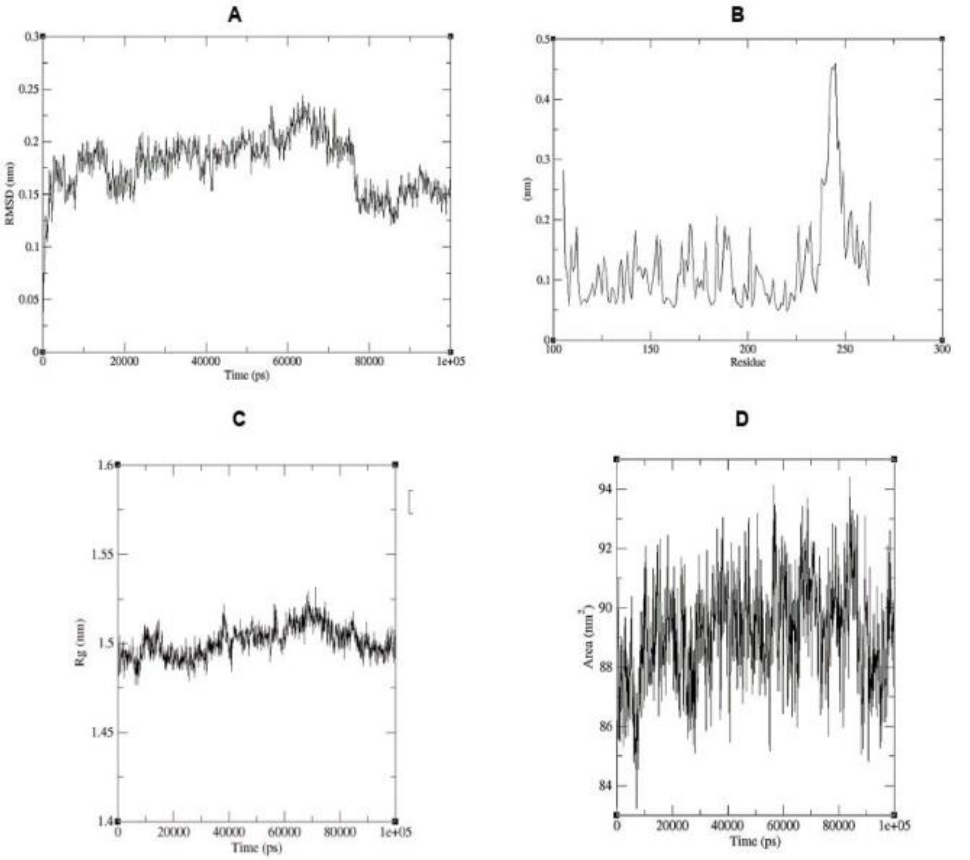

Figure 3. (A) RMSD, (B) RMSF, (C) Rg, (D) SASA of compound (I)-MMP-10 (PDB ID: 1Q3A) complex during 100 ns MD simulation.

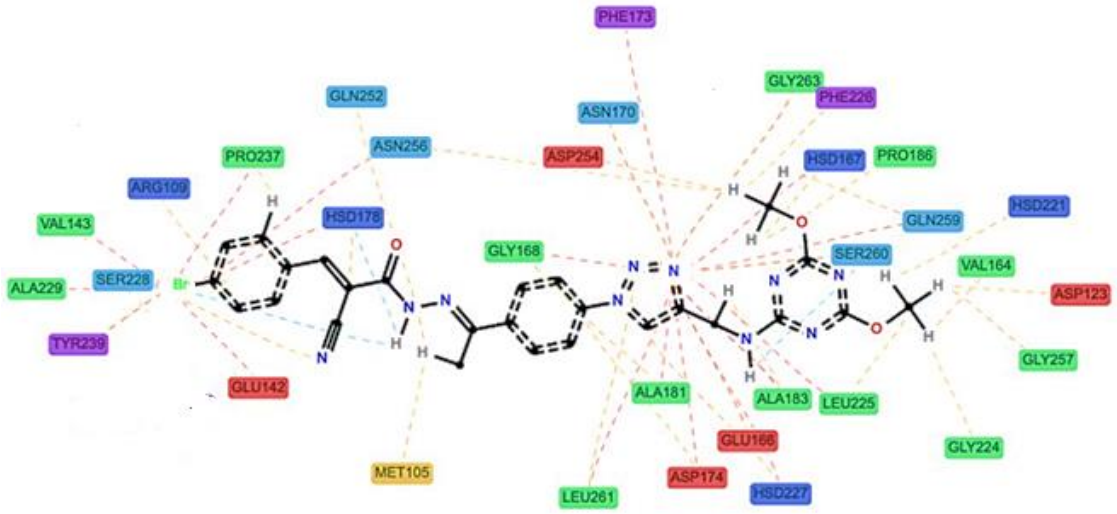

Figure 4. Ligand-protein 2D interactions of compound (**I**)-MMP-10 (PDB ID: 1Q3A) complex during 100 ns MD simulation.

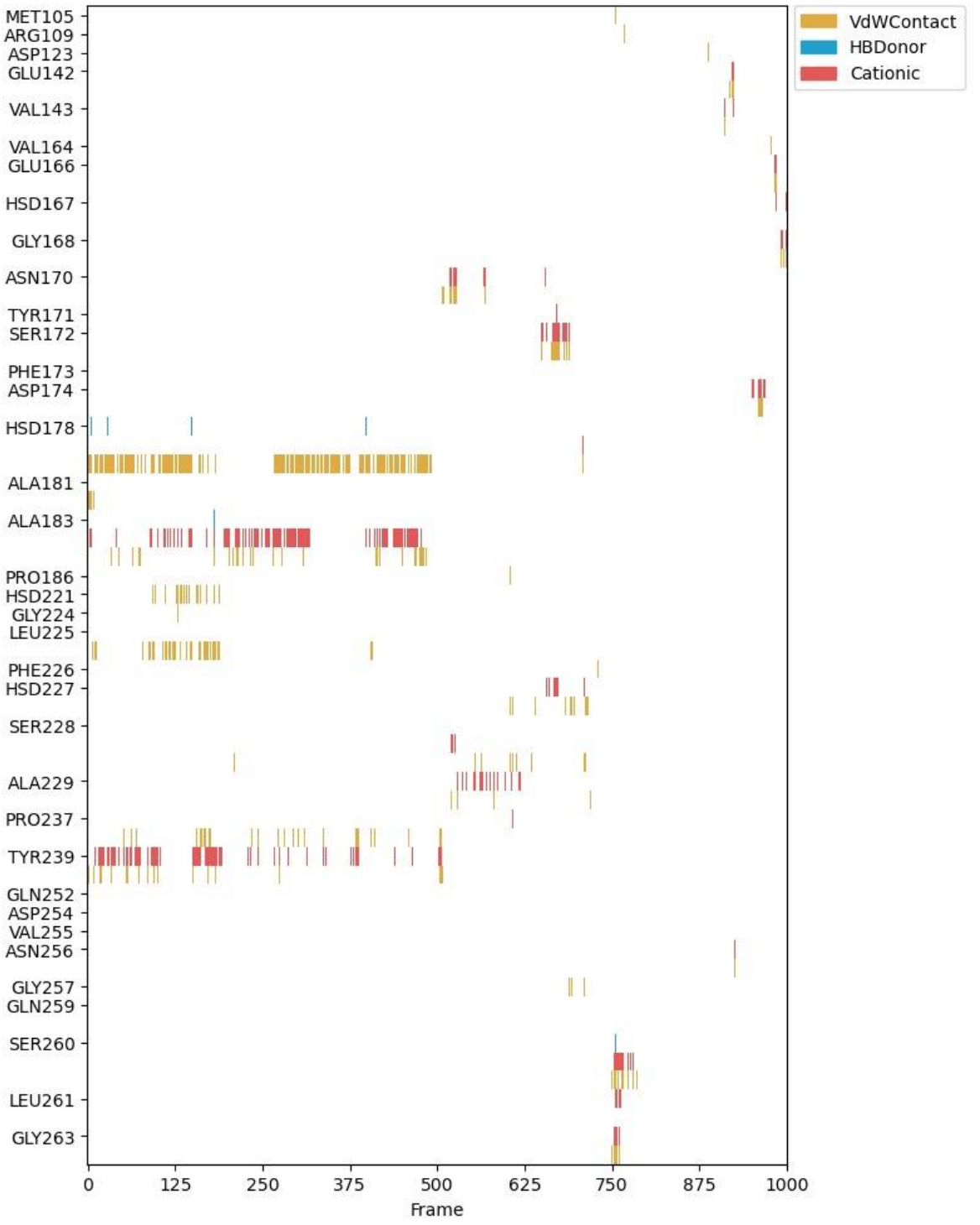

Figure 5. (Contact frequency (CF) analysis of compound (I)-MMP-10 (PDB ID: 1Q3A) complex during 100 ns MD simulation.

Table 1. The calculated binding free energies (kcal/mol) of the simulated compound (I)-MMP-10 (PDB ID: 1Q3A).

Complex	ΔG	Van der Waal energy	Electrostatic energy	Polar solvation energy
(I)-1Q3A	-5.87±2.74	-26.25±1.41	-16.38±0.12	36.76±18.87

References

[1] Karplus, M.; McCammon, J. A. Molecular Dynamics Simulations of Biomolecules. Nat. Struct. Biol. 2002, 9(9), 646–652.
[2] Spahn, V.; Del Vecchio, G.; Labuz, D.; Rodriguez-Gaztelumendi, A.; Massaly, N.; Temp, J.; Durmaz, V.; Sabri, P.; Reidelbach, M.; Machelska, H.; Weber, M.; Stein, C. A. Nontoxic Pain Killer Designed by Modeling of Pathological Receptor Conformations. Science. 2017, 355(6328), 966–969.
[3] Udier-Blagović, M.; Tirado-Rives, J.; Jorgensen, W. L. Validation of a Model for the Complex of HIV-1 Reverse Transcriptase with Nonnucleoside Inhibitor TMC125. J. Am. Chem. Soc. 2003, 125(20), 6016–6017.
[4] Perez, A.; Morrone, J. A.; Simmerling, C.; Dill, K. A. Advances in Free-Energy-Based Simulations of Protein Folding and Ligand Binding. Curr. Opin. Struct. Biol. 2016, 36, 25–31.
[5] Hou, T.; Wang, J.; Li, Y.; Wang, W. Assessing the Performance of the MM/PBSA and MM/GBSA Methods. 1. The Accuracy of Binding Free Energy Calculations Based on Molecular Dynamics Simulations. J. Chem. Inf. Model. 2011, 51(1), 69–82.
[6] Salo-Ahen, O. M. H.; Alanko, I.; Bhadane, R.; Bonvin, A. M. J. J.; Honorato, R. V.; Hossain, S.; Juffer, A. H.; Kabedev, A.; Lahtela-Kakkonen, M.; Larsen, A. S.; Lescrinier, E.; Marimuthu, P.; Mirza, M. U.; Mustafa, G.; Nunes-Alves, A.; Pantsar, T.; Saadabadi, A.; Singaravelu, K.; Vanmeert, M. Molecular Dynamics Simulations in Drug Discovery and Pharmaceutical Development. Processes. 2020, 9(1), 71, 2–60.
[7] Stetler-Stevenson, W. G.; Aznavoorian, S.; Liotta, L. A. Tumor cell interactions with the extracellular matrix during invasion and metastasis. Annu. Rev. Cell Biol. 1993, 9, 541–573.
[8] Walker, C.; Mojares, E.; Del Río Hernández, A. Role of Extracellular Matrix in Development and Cancer Progression. Int. J. Mol. Sci. 2018, 19(10), 3028–3058.
[9] Kessenbrock, K.; Plaks, V.; Werb, Z. Matrix Metalloproteinases: Regulators of the Tumor Microenvironment. Cell. 2010, 141(1), 52–67.
[10] Cathcart, J.; Pulkoski-Gross, A.; Cao, J. Targeting Matrix Metalloproteinases in Cancer: Bringing New Life to Old Ideas. Genes Dis. 2015, 2(1), 26–34.
[11] Curran, S.; Dundas, S. R.; Buxton, J.; Leeman, M. F.; Ramsay, R.; Murray, G. I. Matrix Metalloproteinase/Tissue Inhibitors of Matrix Metalloproteinase Phenotype Identifies Poor Prognosis Colorectal Cancers. Clinical Cancer Research. 2004, 10(24), 8229–8234.
[12] Forget, M.-A.; Desrosiers, R. R.; Béliveau, R. Physiological Roles of Matrix Metalloproteinases: Implications for Tumor Growth and Metastasis. Can. J. Physiol. Pharmacol. 1999, 77(7), 465–480.
[13] Visse, R.; Nagase, H. Matrix Metalloproteinases and Tissue Inhibitors of Metalloproteinases. Circ. Res. 2003, 92(8), 827–839.
[14] Maskos, K. Crystal Structures of MMPs in Complex with Physiological and Pharmacological Inhibitors. Biochimie. 2005, 87(3–4), 249–263.
[15] Schechter, I.; Berger, A. On the Size of the Active Site in Proteases. I. Papain. Biochem. Biophys. Res. Commun. 1967, 27(2), 157–162.
[16] Bhowmick, N. A.; Neilson, E. G.; Moses, H. L. Stromal Fibroblasts in Cancer Initiation and Progression. Nature. 2004, 432, 332–337.
[17] Chambers, A. F.; Matrisian, L. M. Changing Views of the Role of Matrix Metalloproteinases in Metastasis. JNCI Journal of the National Cancer Institute. 1997, 89(17), 1260–1270.
[18] Kalluri, R.; Zeisberg, M. Fibroblasts in Cancer. Nat. Rev. Cancer. 2006, 6(5), 392–401.
[19] Brown, S.; Meroueh, S.; Fridman, R.; Mobashery, S. Quest for Selectivity in Inhibition of Matrix Metalloproteinases. Curr. Top. Med. Chem. 2004, 4(12), 1227–1238.
[20] Nuti, E.; Tuccinardi, T.; Rossello, A. Matrix Metalloproteinase Inhibitors: New Challenges in the Era of Post Broad-Spectrum Inhibitors. Curr. Pharmaceut. Des. 2007, 13, 2087–2100.
[21] Georgiadis, D.; Yiotakis, A. Specific Targeting of Metzincin Family Members with Small-Molecule Inhibitors: Progress toward a Multifarious Challenge. Bioorganic and Medicinal Chemistry. 2008, 16, 8781–8794.
[22] Rao, B. G. Recent Developments in the Design of Specific Matrix Metalloproteinase Inhibitors Aided by Structural and Computational Studies. Curr. Pharmaceut. Des. 2005, 11, 295–322.
[23] Coussens, L. M.; Fingleton, B.; Matrisian, L. M. Matrix Metalloproteinase Inhibitors and Cancer—Trials and Tribulations. Science. 2002, 295(5564), 2387–2392.
[24] Breuer, E.; Frant, J.; Reich, R. Recent Non-Hydroxamate Matrix Metalloproteinase Inhibitors. Expert Opinion on Therapeutic Patents. 2005, 15, 253–269.
[25] Whittaker, M.; Floyd, C. D.; Brown, P.; Gearing, A. J. Design and Therapeutic Application of Matrix

Metalloproteinase Inhibitors. Chem. Rev. 1999, 99(9), 2735–2776.

[26] Overall, C. M.; Kleifeld, O. Tumour Microenvironment - Opinion: Validating Matrix Metalloproteinases as Drug Targets and Anti-Targets for Cancer Therapy. Nat. Rev. Cancer. 2006, 6(3), 227–239.

[27] Jacobsen, J. A.; Major Jourden, J. L.; Miller, M. T.; Cohen, S. M. To Bind Zinc or Not to Bind Zinc: An Examination of Innovative Approaches to Improved Metalloproteinase Inhibition. Biochimica et Biophysica Acta (BBA) - Molecular Cell Research. 2010, 1803, 72–94.

[28] El Ashry, E. S. H.; Awad, L. F.; Teleb, M.; Ibrahim, N. A.; Abu-Serie, M. M.; Abd Al Moaty, M. N. Structure-Based Design and Optimization of Pyrimidine- and 1,2,4-Triazolo[4,3-a]Pyrimidine-Based Matrix Metalloproteinase-10/13 Inhibitors via Dimroth Rearrangement towards Targeted Polypharmacology. Bioorg. Chem. 2020, 96, 103616.

[29] Senn, N.; Ott, M.; Lanz, J.; Riedl, R. Targeted Polypharmacology: Discovery of a Highly Potent Non-Hydroxamate Dual Matrix Metalloproteinase (MMP)-10/-13 Inhibitor. J. Med. Chem. 2017, 60(23), 9585–9598.

[30] Gill, J. H.; Kirwan, I. G.; Seargent, J. M.; Martin, S. W.; Tijani, S.; Anikin, V. A.; Mearns, A. J.; Bibby, M. C.; Anthoney, A.; Loadman, P. M. MMP-10 Is Overexpressed, Proteolytically Active, and a Potential Target for Therapeutic Intervention in Human Lung Carcinomas. Neoplasia. 2004, 6(6), 777–785.

[31] Deraz, E. M.; Kudo, Y.; Yoshida, M.; Obayashi, M.; Tsunematsu, T.; Tani, H.; Siriwardena, S. B. S. M.; Kiekhaee, M. R.; Qi, G.; Iizuka, S.; Ogawa, I.; Campisi, G.; Muzio, L. L.; Abiko, Y.; Kikuchi, A.; Takata, T. MMP-10/Stromelysin-2 Promotes Invasion of Head and Neck Cancer. PLoS One. 2011, 6(10), e25438.

[32] Leeman, M. F.; Curran, S.; Murray, G. I. The Structure, Regulation, and Function of Human Matrix Metalloproteinase-13. Crit. Rev. Biochem. Mol. Biol. 2002, 37(3), 149–166.

[33] Mathew, R.; Khanna, R.; Kumar, R.; Mathur, M.; Shukla, N. K.; Ralhan, R. Stromelysin-2 Overexpression in Human Esophageal Squamous Cell Carcinoma: Potential Clinical Implications. Cancer Detect. Prev. 2002, 26(3), 222–228.

[34] Tardif, G.; Reboul, P.; Pelletier, J.-P.; Martel-Pelletier, J. Ten Years in the Life of an Enzyme: The Story of the Human MMP-13 (Collagenase-3). Mod. Rheumatol. 2004, 14(3), 197–204.

[35] Barksby, H. E.; Milner, J. M.; Patterson, A. M.; Peake, N. J.; Hui, W.; Robson, T.; Lakey, R.; Middleton, J.; Cawston, T. E.; Richards, C. D.; Rowan, A. D. Matrix Metalloproteinase 10 Promotion of Collagenolysis via Procollagenase Activation: Implications for Cartilage Degradation in Arthritis. Arthritis Rheum. 2006, 54(10), 3244–3253.

[36] Li, N.-G.; Shi, Z.-H.; Tang, Y.-P.; Wang, Z.-J.; Song, S.-L.; Qian, L.-H.; Qian, D.-W.; Duan, J.-A. New Hope for the Treatment of Osteoarthritis Through Selective Inhibition of MMP-13. Curr. Med. Chem. 2011, 18(7), 977–1001.

[37] Quillard, T.; Tesmenitsky, Y.; Croce, K.; Travers, R.; Shvartz, E.; Koskinas, K. C.; Sukhova, G. K.; Aikawa, E.; Aikawa, M.; Libby, P. Selective Inhibition of Matrix Metalloproteinase-13 Increases Collagen Content of Established Mouse Atherosclerosis. Arterioscler. Thromb. Vasc. Biol. 2011, 31(11), 2464–2472.

[38] Paumier, J. M.; Thinakaran, G. Matrix Metalloproteinase 13, a New Target for Therapy in Alzheimer's Disease. Genes and Diseases. 2019, 6(1), 1–2.

[39] Morcos, C. A.; Khattab, S. N.; Haiba, N. S.; Bassily, R. W.; Abu-Serie, M. M.; Teleb, M. Battling Colorectal Cancer via S-Triazine-Based MMP-10/13 Inhibitors Armed with Electrophilic Warheads for Concomitant Ferroptosis Induction; the First-in-Class Dual-Acting Agents. Bioorg. Chem. 2023, 141, 106839.

[40] Molecular Operating Environment (MOE) 2019.0102. Chemical Computing Group Inc.: Montreal, QC, Canada.

[41] Bertini, I.; Calderone, V.; Fragai, M.; Luchinat, C.; Mangani, S.; Terni, B. Crystal Structure of the Catalytic Domain of Human Matrix Metalloproteinase 10. J. Mol. Biol. 2004, 336(3), 707–716.

[42] GROMACS: fast, flexible, free. http://www.gromacs.org/. Accessed 25 August 2023.

[43] Jo, S.; Kim, T.; Iyer, V. G.; Im, W. CHARMM-GUI: A Web-based Graphical User Interface for CHARMM. J. Comput. Chem. 2008, 29(11), 1859–1865.

[44] Brooks, B. R.; Brooks, C. L.; Mackerell, A. D.; Nilsson, L.; Petrella, R. J.; Roux, B.; Won, Y.; Archontis, G.; Bartels, C.; Boresch, S.; Caflisch, A.; Caves, L.; Cui, Q.; Dinner, A. R.; Feig, M.; Fischer, S.; Gao, J.; Hodoscek, M.; Im, W.; Kuczera, K.; Lazaridis, T.; Ma, J.; Ovchinnikov, V.; Paci, E.; Pastor, R. W.; Post, C. B.; Pu, J. Z.; Schaefer, M.; Tidor, B.; Venable, R. M.; Woodcock, H. L.; Wu, X.; Yang, W.; York, D. M.; Karplus, M. CHARMM: The Biomolecular Simulation Program. J. Comput. Chem. 2009, 30(10), 1545–1614.

[45] Lee, J.; Cheng, X.; Swails, J. M.; Yeom, M. S.; Eastman, P. K.; Lemkul, J. A.; Wei, S.; Buckner, J.; Jeong, J. C.; Qi, Y.; Jo, S.; Pande, V. S.; Case, D. A.; Brooks, C. L.; MacKerell, A. D.; Klauda, J. B.; Im, W. CHARMM-GUI Input Generator for NAMD, GROMACS, AMBER, OpenMM, and CHARMM/OpenMM Simulations Using the CHARMM36 Additive Force Field. J. Chem. Theory Comput. 2016, 12(1), 405–413.